1.B

Nuclear Physics A319 (1979) 1–20; © *North-Holland Publishing Co., Amsterdam*

PERTURBATIONAL CALCULATIONS OF n-d BREAKUP FOR REALISTIC POTENTIALS

C. STOLK and J. A. TJON

Instituut voor Theoretische Fysica der Rijksuniversiteit, Utrecht, The Netherlands

Received 13 December 1978

Abstract: The perturbational scheme used previously to calculate the elastic n-d scattering is extended to the case of breaking scattering. Results are presented at 22.7 MeV and 46.3 MeV, for the Reid soft core potential, the Graz potential and the Y-Y_7-P_{DOL} potential. Significant differences are found between these potentials.

1. Introduction

In most research done on the three-nucleon system it is hoped implicitly or explicitly that it will prove possible to extract information on the N-N interaction from the three-particle system, since it is the simplest system that depends on the off-shell parts of the two-nucleon transition matrix. Although calculations with simple local or separable s-wave potentials [1–4]) and with the boundary condition model [5]) have shown that at lower energies off-shell effects in the cross sections may be small, it has also been shown that at higher energies off-shell effects do exist [6]). Moreover for noncentral potentials the polarizations open a new class of observables which until recently received very little attention. In the work at 22.7 MeV with the Y-Y_7-P_{DOL} potential [7,8]) indeed significant effects of noncentral components in the force were found, both in the cross sections and in the polarization observables; it is therefore worthwhile to create a framework for the study of the three-nucleon system with more general potentials, and in particular with a local potential with the one pion exchange tail. In a previous paper, hereafter referred to as ST [9]) †, we developed a framework for the elastic n-d scattering and presented results for the Reid soft core (RSC) potential; in this paper we extend this work to the n-d breakup scattering.

The plan of this paper is as follows. In the next section the perturbation formalism of ST is extended to the breakup scattering. Sect. 3 deals with the three-nucleon observables that we shall study. The discussion of how the actual calculations were performed is given in sect. 4; also some attention is paid to the numerical aspects of the calculations. In sect. 5 we present results at 46.3 MeV for the RSC potential [10]),

† Table 1 and fig. 17 of this paper require some corrections.

the Graz potential [11]) and the Y-Y_7-P_{DOL} potential [7]), and at 22.7 MeV for the RSC potential [10]) and the Y-Y_7-P_{DOL} potential [7]). Finally, some conclusions are drawn in the last section.

Some results have already been published in a letter [12]). A more complete account of the work presented here and in ST is given in ref. [13]).

2. Perturbational treatment of the breakup amplitude

For the notation and the derivation of the perturbational expressions we refer to ST. The breakup amplitude for the scattering of a n-d state $|\alpha \boldsymbol{q}_i \beta_i\rangle$ into a state $|f\beta_f\rangle$ (f for the outgoing single-particle momenta, β_f for the spins and isospins) is given by

$$M(f\beta_f|\boldsymbol{q}_i\beta_i) = \sqrt{\tfrac{1}{2}}\sum_k \sum_{\Gamma_i\Gamma} \int \mathrm{d}p p^2 \mathrm{d}q q^2 \langle f\beta_f|pq\Gamma\rangle_k U_i(pq\Gamma)_2\langle \alpha\bar{q}\Gamma_i|\alpha \boldsymbol{q}_i\beta_i\rangle_2. \tag{2.1}$$

Here the integrations are purely formal, since the matrix elements $\langle f\beta_f|pq\Gamma\rangle_k$ contain delta functions that express p and q in the momenta of the outgoing free particles. The integral equation for the wave function U is given in ST; it is

$$\begin{aligned} U_i(pq\Gamma) \equiv U(pq\Gamma|\alpha\bar{q}\Gamma_i) &= 4_2\langle p\bar{q}\Gamma|T_2(s+i\varepsilon)|\alpha\bar{q}\Gamma_i\rangle_1 \\ &\quad -2\sum_{\Gamma'}{}' \int \frac{\mathrm{d}p'\mathrm{d}q'p'^2q'^2}{p'^2+q'^2-s-i\varepsilon}\, {}_2\langle pq\Gamma|T_2(s+i\varepsilon)|p'q'\Gamma'\rangle_1 U_i(p'q'\Gamma'). \end{aligned} \tag{2.2}$$

The perturbational scheme consists of writing the two-body T-matrix and the deuteron wave function as

$$\begin{aligned} T_2 &= T_2^{(0)} + \delta T_2^{(1)}, \\ |\alpha\rangle &= |\alpha^{(0)}\rangle + \delta|\alpha^{(1)}\rangle, \end{aligned} \tag{2.3}$$

where the terms with δ are considered to be small. Expanding in δ, we find as a result that the wave function up to first order can be written as

$$U_i(pq\Gamma) = U_i^{(0)}(pq\Gamma) + \delta U_i^{(1)}(pq\Gamma) + \mathrm{O}(\delta^2), \tag{2.4}$$

with

$$\begin{aligned} U_i^{(1)}(pq\Gamma) &= 4_2\langle pq\Gamma|T_2^{(0)}|\alpha^{(1)}\bar{q}\Gamma_i\rangle_1 + 4_2\langle pq\Gamma|T_2^{(1)}|\alpha^{(0)}\bar{q}\Gamma_i\rangle_1 \\ &\quad -2\sum_{\Gamma'}{}' \int \frac{\mathrm{d}p'\mathrm{d}q'p'^2q'^2}{p'^2+q'^2-s-i\varepsilon}\, {}_2\langle pq\Gamma|T_2^{(1)}|p'q'\Gamma'\rangle_1 U_i^{(0)}(p'q'\Gamma') \\ &\quad -2\sum_{\Gamma'}{}' \int \frac{\mathrm{d}p'\mathrm{d}q'p'^2q'^2}{p'^2+q'^2-s-i\varepsilon}\, {}_2\langle pq\Gamma|T_2^{(0)}|p'q'\Gamma'\rangle_1 U_i^{(1)}(p'q'\Gamma'), \end{aligned} \tag{2.5}$$

while $U_i^{(0)}$ satisfies the same equation (2.2) with α replaced by $\alpha^{(0)}$, U by $U^{(0)}$ and T_2 by $T_2^{(0)}$. From eq. (2.5) we see that $U^{(1)}$ satisfies an integral equation with the same kernel as the one for $U^{(0)}$ but with a more complicated inhomogeneous term. In the present case the function $U^{(1)}$ is needed explicitly; it is solved from (2.5) by the same Padé techniques used for $U^{(0)}$. The perturbational contributions to the elastic scattering matrix elements can be obtained by eq. (2.11) of ST; however since $U^{(1)}$ is available, they are obtained more simply as

$$\begin{aligned} M(\Gamma_f|\Gamma_i) = {} & 2\,{}_1\langle\alpha^{(0)}\bar{q}\Gamma_f|(s-H_0)|\alpha^{(1)}\bar{q}\Gamma_i\rangle_2 + 2\,{}_1\langle\alpha^{(1)}\bar{q}\Gamma_f|(s-H_0)|\alpha^{(0)}\bar{q}\Gamma_i\rangle_2 \\ & + \sum_\Gamma \int \mathrm{d}p p^2 \mathrm{d}q q^2\, {}_1\langle\alpha^{(1)}\bar{q}\Gamma_f|pq\Gamma\rangle_2 U_i^{(0)}(pq\Gamma) \\ & + \sum_\Gamma \int \mathrm{d}p p^2 \mathrm{d}q q^2\, {}_1\langle\alpha^{(0)}\bar{q}\Gamma_f|pq\Gamma\rangle_2 U_i^{(1)}(pq\Gamma). \end{aligned} \tag{2.6}$$

In the actual calculations we used the K-matrix formalism given in sect. 4 of ST; the perturbation was calculated for the function $W(pq\Gamma'|\alpha\bar{q}\Gamma)$ introduced there, and with the aid of the corresponding elastic amplitude $K(\Gamma|\Gamma_i)$ the function $U_i(pq\Gamma)$ was obtained.

3. Observables

From the transition matrix for the breakup scattering the cross sections are found directly by

$$\begin{aligned} \mathrm{d}\sigma = {} & \frac{3\pi^4}{m\bar{q}} \sum_{\beta_f\beta_f'} \delta_{\beta_f\beta_f'} \sum_{\beta_i\beta_i'} M_0(f\beta_f|\boldsymbol{q}_i\beta_i) \\ & \times \langle\alpha\boldsymbol{q}_i\beta_i|\rho_{in}|\alpha\boldsymbol{q}_i\beta_i'\rangle M_0^*(f\beta_f'|\boldsymbol{q}_i\beta_i')\delta(p_n^2+q_n^2-s)\mathrm{d}^3p_n\mathrm{d}^3q_n. \end{aligned} \tag{3.1}$$

Here s is the total energy; p_n and q_n are the relative momenta in the final state with particle n in the special role. Which n is chosen is determined by convenience in the transformation of the volume element for a particular crosssection. If only one particle is detected we have

$$\delta(p_1^2+q_1^2-s)\mathrm{d}^3p_1\mathrm{d}^3q_1 = \tfrac{3}{8}\sqrt{\tfrac{3}{2}}p_1\mathrm{d}\Omega_{p_1}k_1\sqrt{\hbar^2/m}\mathrm{d}E_1\mathrm{d}\Omega_{k_1}, \tag{3.2}$$

and for a kinematically complete experiment we find

$$\delta(p_1^2+q_1^2-s)\mathrm{d}^3p_1\mathrm{d}^3q_1 = \tfrac{3}{4}\sqrt{3}E_2\frac{k_1k_2}{|\boldsymbol{k}_2\cdot(\boldsymbol{k}_2-\boldsymbol{k}_3)|}\mathrm{d}\Omega_{k_2}\mathrm{d}\Omega_{k_1}\mathrm{d}E_1. \tag{3.3}$$

Here the single particle energies E_i and momenta k_i must all be given in the same

frame of reference, but this need not be the c.m. frame, and in particular it may be the lab frame.

In eq. (3.1) ρ_{in} is the density matrix for the incoming beam [14]. The analyzing powers are obtained in the usual way. For the deuteron analyzing powers we always use the irreducible tensor components; in some cases we shall tacitly invoke space reflection symmetry to derive these spherical components from the data for the Cartesian components. Moreover they are treated as target analyzing powers, and hence given in the same axes system as the neutron (projectile) analyzing powers.

To obtain the outgoing polarizations the factor $\delta_{\beta_f\beta_f'}$ in eq. (3.1) should be replaced by the appropriate spin operator, The choice of the axes system is fixed by the Madison convention [15] as far as possible; in the case where two outgoing particles are detected we specify the azimuthal angle of one of the outgoing particles.

We number the particles in the order in which they appear in the descriptor of the reaction, e.g. d(n, nnp). The angles θ_i and ϕ_i are the usual polar angles in the lab frame, the projectile having $\theta_2 = 0$. The angle ϕ_{ij} is the difference in the azimuthal angles of particles i and j, while E_{ij} is the energy associated with the relative motion of these particles.

4. Calculations and accuracy

The determination of the S-matrix elements proceeds in the same manner as in ST, with the single difference that instead of (the K-matrix equivalent of) eq. (2.11) of ST we use eq. (2.6) for the elastic K-matrix.

For the present calculation the function $U_1^{(1)}$ is needed in the last term of eq. (2.6) and in eq. (2.1); we note that in eq. (2.1) we require only those p and q that satisfy the on-energy-shell condition. For this reason we do not calculate the complete function $U_1^{(1)}(pq\Gamma)$, but iterate eq. (2.5) and for each iteration calculate the on-shell function and the integral as in the last term of (2.6); the final results are then found as the Padé approximants to the series obtained. The order of the Padé approximants is chosen the same as in the unperturbed part of the calculation.

However different truncations were made in the partial wave expansions for the perturbational and the unperturbed parts. We never go beyond $l_1 = 5$ (contained in Γ_1 or Γ) for the perturbational terms or beyond $l_1 = 10$ for the unperturbed terms; we ignore $U_1^{(0)}(pq\Gamma)$ for $l_1 > 5$ in the calculation of $M^{(0)}(\Gamma|\Gamma_i)$, and for $l_1 > 3$ in the calculation of $U_1^{(1)}(pq\Gamma)$ and $M^{(1)}(\Gamma|\Gamma_i)$; and in the calculation of $U_1^{(1)}(pq\Gamma)$ we use only the inhomogeneous term in eq. (2.5) when Γ has $l_1 > 3$. These truncations are estimated to introduce errors smaller than those from other numerical sources. Table 1 gives an idea of the overall numerical stability, reflected in the lower elastic phase parameters for different methods of calculation. Some of these numbers are seen to deviate slightly from the corresponding numbers in table 1 of ST; this is because of an improvement in the algorithm and because the second column of table 1 in ST incorrectly also contains the d-wave forces.

TABLE 1

Split phase parameters at 22.7 MeV for two potentials (Reid S+T+P and Y-Y_7-P_{DOL}) and various methods of calculation

	Reid T	Reid K_1	Reid K_2	Y-Y_7-P_{DOL} K_2	Y-Y_7-P_{DOL} X
${}^2\delta^0_{1/2}$	$1.218+0.394i$	$1.236+0.325i$	$1.249+0.320i$	$1.429+0.455i$	$1.421+0.487i$
${}^4\delta^2_{1/2}$	$-0.131+0.051i$	$-0.133+0.040i$	$-0.133+0.040i$	$-0.065+0.058i$	$-0.072+0.043i$
$\eta^+_{1/2}$	$-0.005+0.007i$	$-0.001+0.002i$	$0.000+0.002i$	$-0.034-0.051i$	$-0.039-0.058i$
${}^4\delta^1_{1/2}$	$0.698+0.072i$	$0.688+0.119i$	$0.680+0.117i$	$0.662+0.120i$	$0.697+0.102i$
${}^2\delta^1_{1/2}$	$0.090+0.086i$	$0.016+0.168i$	$0.010+0.161i$	$-0.081+0.192i$	$-0.017+0.182i$
$\varepsilon^-_{1/2}$	$0.641+0.105i$	$0.637+0.109i$	$0.620+0.102i$	$0.585+0.101i$	$0.560+0.104i$
${}^4\delta^0_{3/2}$	$1.118+0.076i$	$1.120+0.036i$	$1.126+0.035i$	$1.154+0.052i$	$1.143+0.054i$
${}^2\delta^2_{3/2}$	$0.110+0.042i$	$0.109+0.038i$	$0.109+0.038i$	$0.091+0.045i$	$0.118+0.049i$
${}^4\delta^2_{3/2}$	$-0.174+0.026i$	$-0.200+0.034i$	$-0.200+0.034i$	$-0.236+0.040i$	$-0.144+0.023i$
$\varepsilon^+_{3/2}$	$0.027-0.000i$	$0.053+0.003i$	$0.053+0.005i$	$0.082-0.004i$	$-0.073+0.010i$
$\zeta^+_{3/2}$	$0.126+0.003i$	$0.113-0.004i$	$0.114-0.002i$	$0.207-0.025i$	$0.208-0.005i$
$\eta^+_{3/2}$	$-0.051-0.013i$	$-0.043-0.006i$	$-0.043-0.008i$	$-0.103-0.012i$	$-0.119-0.027i$
${}^4\delta^1_{3/2}$	$0.512+0.128i$	$0.516+0.122i$	$0.511+0.117i$	$0.454+0.124i$	$0.480+0.111i$
${}^2\delta^1_{3/2}$	$0.258+0.153i$	$0.248+0.173i$	$0.234+0.169i$	$0.131+0.186i$	$0.118+0.177i$
${}^4\delta^3_{3/2}$	$0.028+0.013i$	$0.029+0.017i$	$0.028+0.017i$	$0.057+0.024i$	$0.059+0.026i$
$\varepsilon^-_{3/2}$	$-0.615-0.232i$	$-0.617-0.230i$	$-0.584-0.207i$	$-0.591-0.210i$	$-0.583-0.172i$
$\zeta^-_{3/2}$	$-0.120+0.034i$	$-0.115+0.073i$	$-0.116+0.074i$	$-0.067+0.150i$	$-0.052+0.162i$
$\eta^-_{3/2}$	$0.143-0.116i$	$0.125-0.149i$	$0.133-0.156i$	$-0.024-0.264i$	$-0.034-0.281i$
${}^4\delta^2_{5/2}$	$-0.187+0.028i$	$-0.187+0.029i$	$-0.187+0.028i$	$-0.196+0.029i$	$-0.199+0.028i$
${}^2\delta^2_{5/2}$	$0.129+0.042i$	$0.129+0.041i$	$0.129+0.042i$	$0.113+0.046i$	$0.113+0.046i$
${}^4\delta^4_{5/2}$	$-0.023+0.002i$	$-0.023+0.002i$	$-0.023+0.002i$	$-0.020+0.003i$	$-0.020+0.002i$
$\varepsilon^+_{5/2}$	$0.030+0.003i$	$0.029+0.002i$	$0.029+0.001i$	$0.039+0.001i$	$0.051+0.000i$
$\zeta^+_{5/2}$	$-0.068-0.009i$	$-0.068-0.003i$	$-0.068-0.003i$	$-0.073+0.006i$	$-0.069+0.008i$
$\eta^+_{5/2}$	$-0.125+0.031i$	$-0.123+0.033i$	$-0.123+0.034i$	$-0.132+0.041i$	$-0.129+0.041i$
${}^4\delta^1_{5/2}$	$0.617+0.075i$	$0.614+0.080i$	$0.616+0.080i$	$0.576+0.076i$	$0.658+0.083i$
${}^2\delta^3_{5/2}$	$-0.023+0.011i$	$-0.023+0.011i$	$-0.023+0.011i$	$-0.023+0.011i$	$-0.024+0.010i$
${}^4\delta^3_{5/2}$	$0.046+0.007i$	$0.046+0.006i$	$0.046+0.006i$	$0.050+0.007i$	$0.046+0.005i$
$\varepsilon^-_{5/2}$	$0.010+0.034i$	$0.007+0.032i$	$0.008+0.032i$	$0.054+0.031i$	$0.039+0.021i$
$\zeta^-_{5/2}$	$0.084-0.018i$	$0.080-0.008i$	$0.079-0.008i$	$0.094-0.001i$	$0.092-0.001i$
$\eta^-_{5/2}$	$-0.028+0.011i$	$-0.026+0.007i$	$-0.026+0.007i$	$-0.035+0.004i$	$-0.033+0.002i$

Numbers are in radians.
Method K_1 uses eq. (2.11) of ST, while method K_2 uses (2.6).
The last column is obtained from the exact calculation [8]).

From the first three columns of table 1 we conclude that in this case the main source of the error in our results is the truncation of the perturbation series at the first order term, as reflected in the difference between the T-matrix and K-matrix results. We recall that at higher energies the perturbational approach seems to give a better convergence, and that the convergence may affect different observables in different ways. Figs. 1 and 2 illustrate this point, showing the effect of a difference in the calculating method on the one hand and in the potential on the other hand.

In the breakup proton spectra there is an effect of numerical origin that requires separate mention. The outgoing wave function is calculated on a finite mesh of values of q, suitable for the integrations; to obtain its value in the points required by

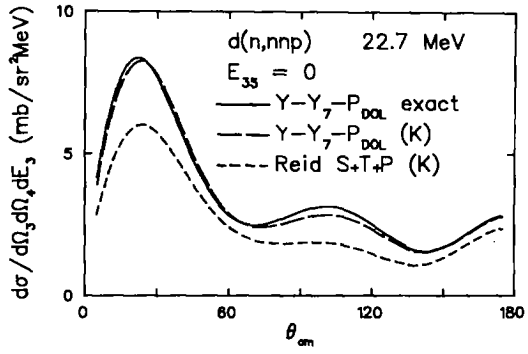

Fig. 1. Breakup differential cross section at 22.7 MeV for FSI for Y-Y_7-P_{DOL} (exact, and perturbation K-matrix) and Reid (s- and p-wave forces and tensor force). $\theta_{c.m.}$ is the c.m. polar angle of particle 4.

eq. (2.1) we use cubic interpolation. If instead of this we use an interpolation procedure that guarantees first derivative continuity, we find slight modifications in some parts of the spectra, viz. in figs. 16–18 just above $E_3 = 40$ MeV and in figs. 20–23 for E_3 between 17 and 19 MeV. Moreover in these regions both interpolation techniques produce small and different oscillations; in figs. 16–18 and figs. 20–23 these have been smoothed out by hand.

5. Results and discussion

Calculations of the breakup scattering were performed at two neutron bombarding energies and for three potentials, viz. 22.7 MeV for the RSC potential [10]) and for

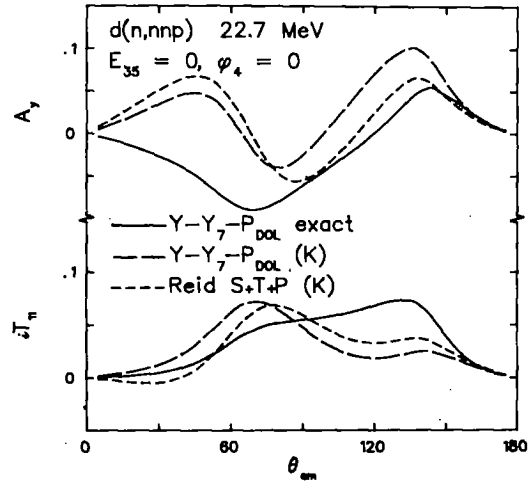

Fig. 2. Breakup analyzing powers at 22.7 MeV for FSI. Curves as in fig. 1.

the Y-Y_7-P_{DOL} potential [7]), and at 46.3 MeV for the RSC potential [10]), the Y-Y_7-P_{DOL} potential [7]) and the Graz potential [11]). We used the same separation of the two-nucleon T-matrix as in ST, i.e. the s-s elements (unperturbed part), the other elements in the $^3S_1$-$^3D_1$ channels (tensor force, also including the deuteron d-wave), the p-p elements (p-wave forces), and the d-d elements in the $^1D_2$ and $^3D_2$ channels (d-wave forces; the $^3D_3$-$^3G_3$ channel is ignored). The deuteron wave function was always normalized to one, whether or not it was taken to contain a d-wave component.

For a given bombarding energy, the kinematics of the outgoing state is completely determined in a given axes system by five continuous variables. One of these is the azimuthal angle corresponding to a rotation of the entire system around the incoming beam; this angle is fixed conventionally or explicitly as mentioned in sect. 3. This leaves us with an essentially four-dimensional phase space. Because of the required computer time we have not been able to perform a systematic search over this entire phase space; we therefore selected certain area's where interesting phenomena are expected. Among these are the final state interaction loci [16,17]) (FSI; the relative energy of two outgoing particles is zero); the quasi-free scattering loci [18]) (QFS; one of the particles has the same velocity vector as it had in the incoming state); the constant-relative-energy loci [19]) (the triangle formed by the relative momenta of the outgoing particles has a prescribed shape and is rotated around the c.m. momentum vector of one of the particles); the symmetric-constant-relative-energy locus [20]) (as the preceding loci, but all relative energies are equal and the triangle is rotated around the relative momentum vector of the two identical particles); the collinearity loci [21]) (in the c.m. frame the outgoing momenta are collinear, and more in particular one of the particles is at rest in the c.m.); and several kinematical loci (the lab angles of two outgoing particles are fixed). For the kinematical loci we have projected the spectra on the E_3 energy axis; in those cases where a given E_3 allows two values of E_4 at the given angles, the results presented never contain the lower E_4 contribution. We verified that this affects the spectra only very close to the maximum E_3, because away from this maximum along the second branch the cross section drops very rapidly to zero.

We also calculated some kinematically incomplete configurations (only one particle is detected at a fixed angle).

In the remainder of this section we first discuss the results obtained at 46.3 MeV for different potentials along some of these loci, and subsequently give some results at 22.7 MeV. The data for the kinematically complete experiments usually are for p-d; Petersen *et al.* [22]) estimate that the Coulomb force probably may be neglected as long as the p-p relative energy is well above 1 MeV. This condition is fulfilled in all cases where we compare our n-d calculations with p-d experiments, except in the high energy region of our proton spectra.

Figs. 3 to 5 show the differential cross section at 46.3 MeV for n-p FSI. Here the single neutron has c.m. angles $\theta_{c.m.}$ and ϕ_4 (= 0). From these figures we see that there are large differences in the results for the three potentials already for the

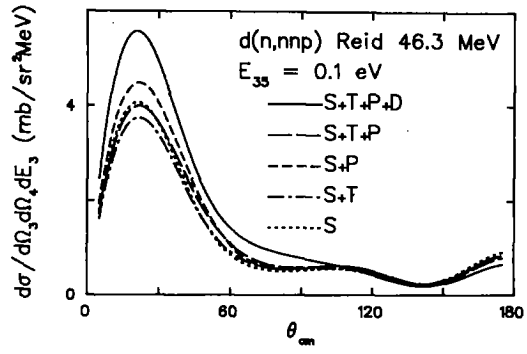

Fig. 3. Breakup differential cross section at 46.3 MeV for FSI for the Reid potential. Curve labels indicate components in the two-nucleon T-matrix. S: s-wave forces. T: tensor force. P: p-wave forces. D: $^1D_2$ and $^3D_2$ forces.

s-wave forces, but also in the perturbational contributions. Moreover, there is a sizable contribution from the d-wave forces. The vector analyzing powers for the same locus, shown in figs. 6 to 8, exhibit rather similar effects of the partial wave forces for the different potentials, the general shape of the curves being determined by the tensor force. Inclusion of the d-wave forces results in a drastic reduction of the neutron analyzing power at angles below $\theta_{c.m.} = 60°$, where the cross section is largest. Among the tensor analyzing powers (figs. 9 to 11) T_{20} shows a strong dependence on all components of the force and on the type of potential used, in particular at angles below 60°. Moreover both T_{20} and the cross section reach large values in this region; therefore an experimental verification should be feasible and could give interesting results. For T_{21} and T_{22} again the tensor force determines the general shape, with strong modifications however from the d-wave forces.

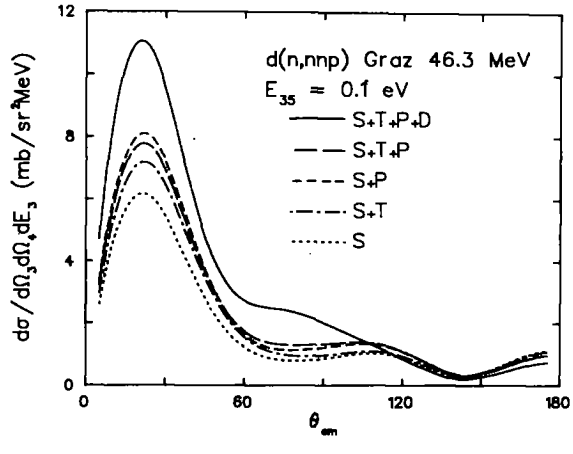

Fig. 4. Breakup differential cross section at 46.3 MeV for FSI for the Graz potential. Curves as in fig. 3.

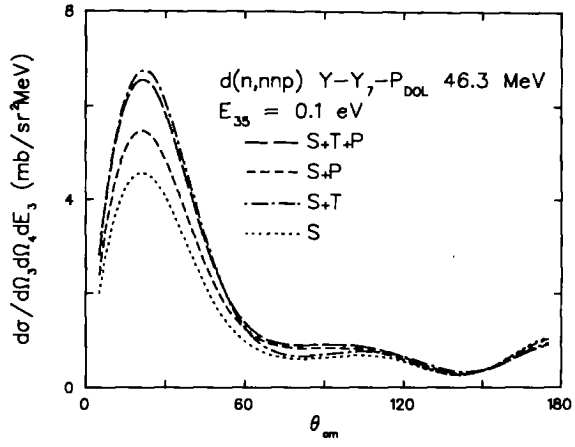

Fig. 5. Breakup differential cross section at 46.3 MeV for FSI for the Y-Y_7-P_{DOL} potential. Curves as in fig. 3.

Figs. 12 and 13 show the n-n QFS locus at 46.3 MeV. There is again a large difference between the results for two potentials already for the s-wave forces. The effect of the tensor force is mainly through the deuteron normalization, and hence smaller for the Graz potential; near the minimum the p- and d-wave forces give a much smaller contribution for the Reid potential.

Fig. 14 shows the symmetric-constant-relative-energy locus. Here the effect of the tensor force is very small; the same is true for the Graz d-wave forces. In view of the symmetry there is a preferred orientation of the axes system, viz. $\phi_5 = 0$. In

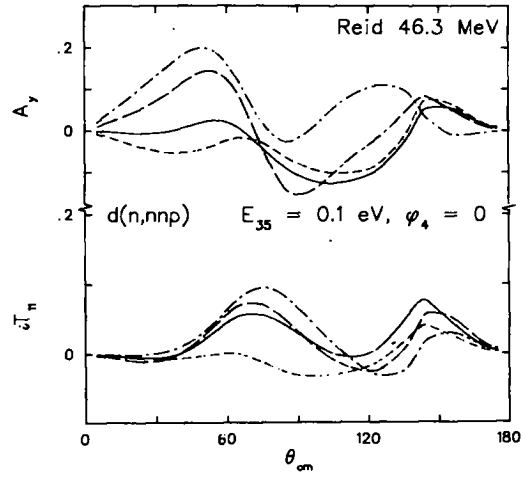

Fig. 6. Vector analyzing powers corresponding to fig. 3.

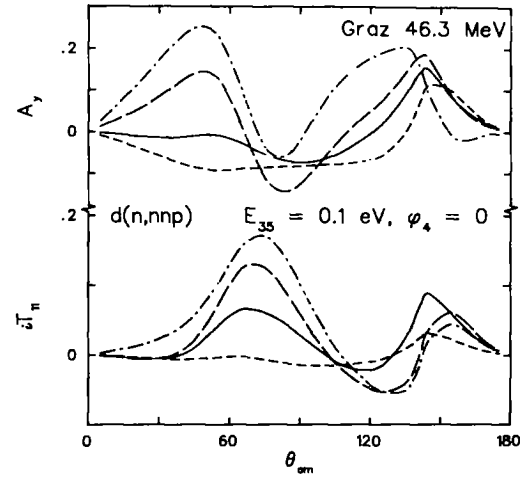

Fig. 7. Vector analyzing powers corresponding to fig. 4.

this system we calculated various analyzing powers; for $E_5 > 5$ MeV they generally are found to be rather small (e.g. -5% to -10% for A_y). Near the minimum of the cross section, the cross section asymmetries (i.e. the products of an analyzing power times the cross section) are smooth functions of the energy E_5, which results in large spikes for the analyzing powers themselves. We made a similar observation for the outgoing polarizations, and we see from fig. 14 that the perturbational contributions to the cross section also are rather smooth functions of E_5. This is

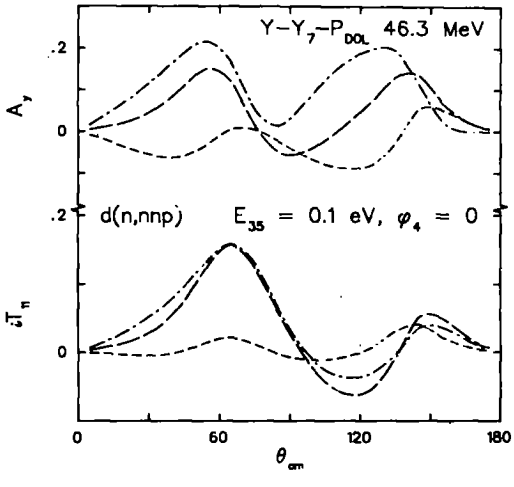

Fig. 8. Vector analyzing powers corresponding to fig. 5.

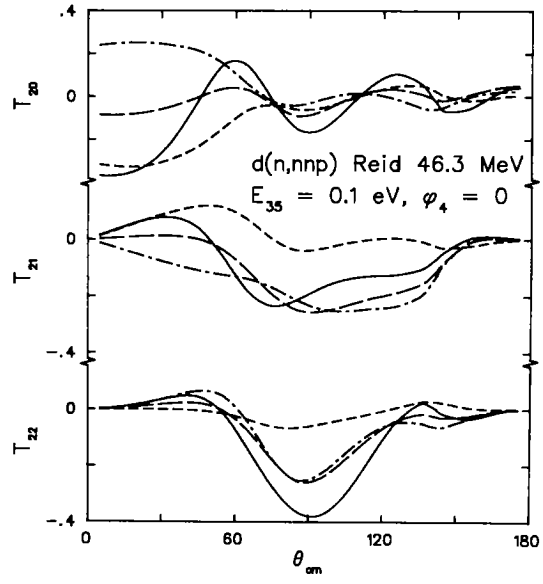

Fig. 9. Deuteron tensor analyzing powers corresponding to fig. 3.

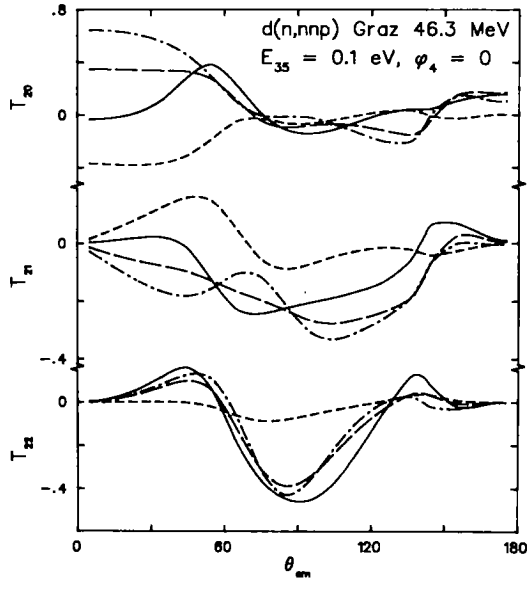

Fig. 10. Deuteron tensor analyzing powers corresponding to fig. 4.

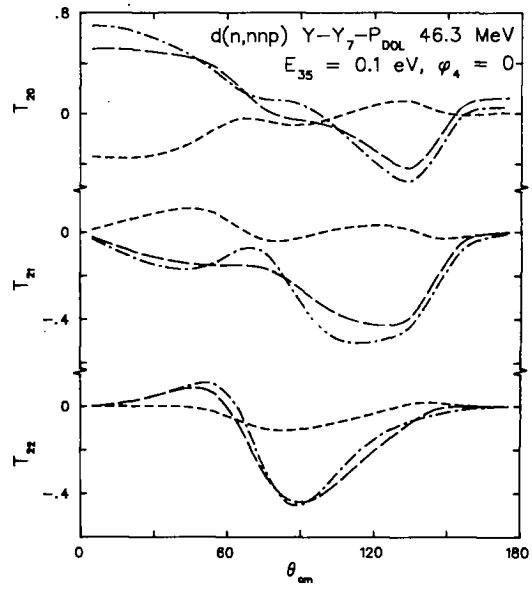

Fig. 11. Deuteron tensor analyzing powers corresponding to fig. 5.

puzzling, because the perturbational contributions to these cross sections consist of cross products between the unperturbed and perturbational amplitudes plus the square of the latter. At the minimum the unperturbed amplitude nearly vanishes, and thus one expects to see the vanishing of the cross product terms. Further analysis however shows, that in this region the cross product terms are approximately purely imaginary, and hence cancel. That the minimum occurs for a variety of s-wave forces is probably only another example of the fact that the scattering is determined

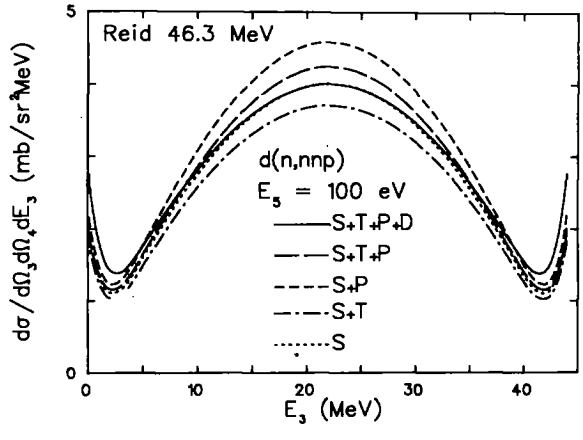

Fig. 12. Breakup differential cross section at 46.3 MeV for QFS for the Reid potential. Curves as in fig. 3.

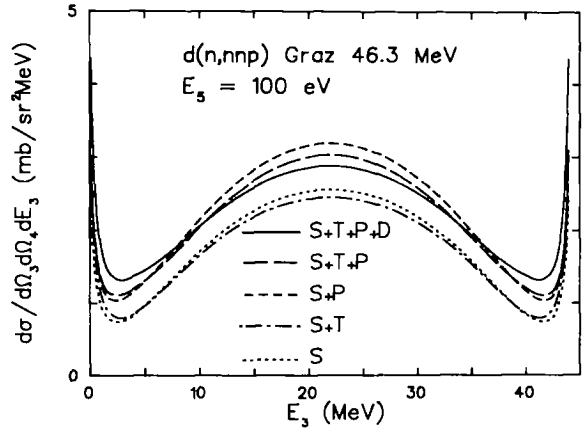

Fig. 13. Breakup differential cross section at 46.3 MeV for QFS for the Graz potential. Curves as in fig. 3.

to a large extent by the low-energy on-shell two-nucleon s-wave force, which is (nearly) the same for any reasonable potential. The p-d data [20]) are at 39.5 MeV; when they are plotted on a slightly extended E_5 axis, the fit to the curve for the full Reid potential is seen to improve.

Fig. 15 shows an example of a coplanar kinematical locus at 46.3 MeV, with p-d data [23]) at 45 MeV. The structure of the cross section curves is determined mainly by the n-p FSI near $E_3 = 2$ MeV ($E_{35} = 0.14$ MeV) and the n-n QFS near $E_3 = 7$ MeV ($E_5 = 0.026$ MeV); from the previous results we see that this leads to large differences between the results for the two potentials. We note that the QFS maxima do not coincide with the minimum E_5, and that the shift is not the same for the

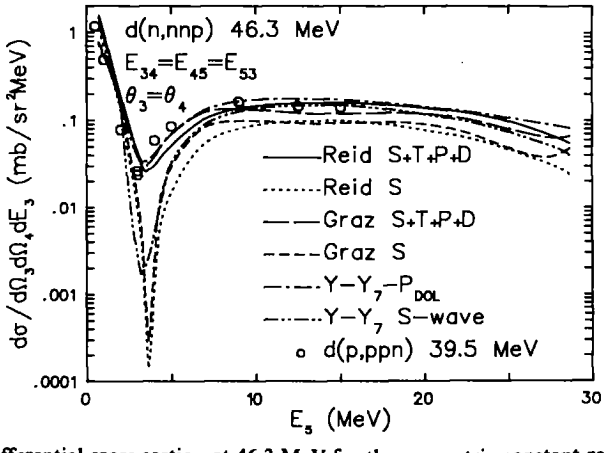

Fig. 14. Breakup differential cross section at 46.3 MeV for the symmetric-constant-relative-energy locus for the full Reid, Graz and Y-Y_7-P_{DOL} potentials and their s-wave truncations.

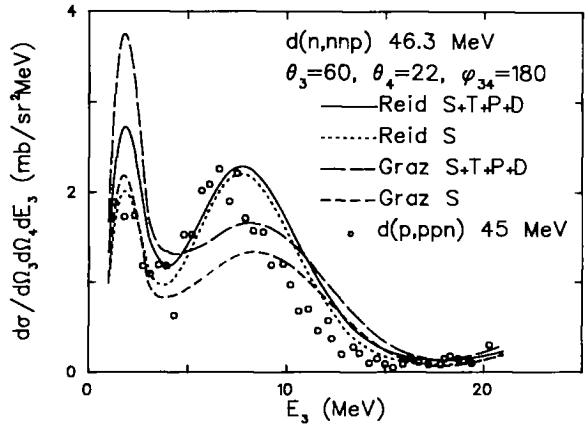

Fig. 15. Breakup differential cross section at 46.3 MeV for $\theta_3 = 60°$, $\theta_4 = 22°$, $\phi_{34} = 180°$, for the full Reid and Graz potentials and their s-wave truncations.

two potentials. Because the shift is determined primarily by the s-wave forces, it seems probable that we have here an interference effect between the FSI and QFS enhancements.

Figs. 16 to 18 show some of the observables for the kinematically incomplete experiment, where only the outgoing protons at a lab angle $\theta_3 = 20°$ are detected. In the differential cross section (fig. 16) the higher partial wave forces contribute strongly near the FSI peak; near the QFS enhancement at 38 MeV they have a smaller but still significant effect. We note that the difference between the results for the two potentials with only s-wave forces is overcompensated by the higher partial wave forces, to which the Graz potential results are much more sensitive.

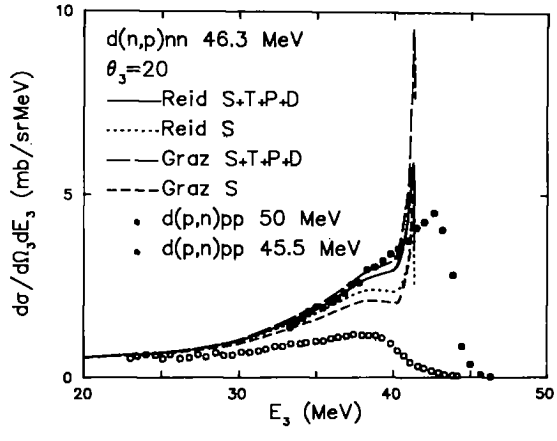

Fig. 16. Breakup differential cross section at 46.3 MeV for the proton spectrum at $\theta_3 = 20°$, for the full Reid and Graz potentials and their s-wave truncations.

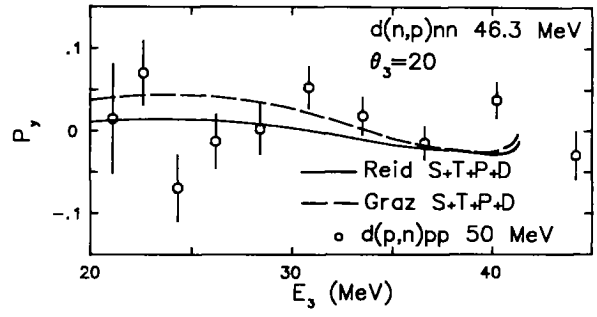

Fig. 17. Proton polarization corresponding to fig. 16.

The two sets of data [24,25]) are inconsistent among themselves. Taking into account the energy resolution of the experiment (about 1 MeV) and the difference in bombarding energy, we expect a reasonable fit to the 50 MeV data. For the polarization of the outgoing proton, shown in fig. 17, we find values well within the scatter of the experimental points [26]) for the charge-conjugated reaction at 50 MeV. Also for both vector analyzing powers (fig. 18) we find small values, in particular in the higher energy region where the cross section is larger.

Next we turn to the results at 22.7 MeV bombarding energy. Fig. 19 shows the n-n QFS locus. In the maximum the Reid d-wave forces contribute negligibly,

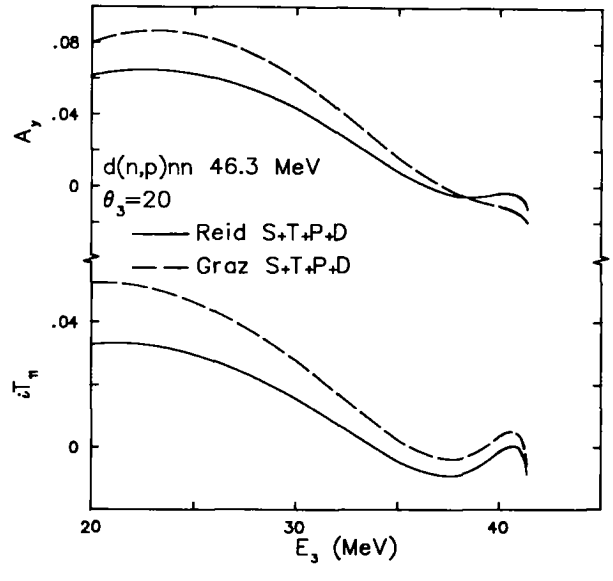

Fig. 18. Vector analyzing powers corresponding to fig. 16.

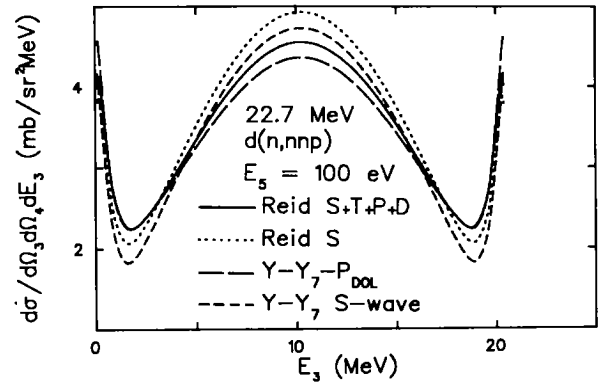

Fig. 19. Breakup differential cross section at 22.7 MeV for QFS for the full Reid and $Y\text{-}Y_7\text{-}P_{DOL}$ potentials and their s-wave truncations.

and the effect of the p-wave forces also is small; the tensor force contributes mainly through the normalization of the deuteron. In the minimum the tensor force contributes are small for the separable potential, but for the Reid potential all components of the force give significant contributions (the tensor force negative, the others positive).

Finally figs. 20 to 23 show results for a kinematically incomplete situation, the proton spectrum at $\theta_3 = 18°$. The data [27]) for the cross section (fig. 20) are at the slightly lower energy of 21.9 MeV, and for p-d. The discrepancy for the last experimental point can be attributed to the different energy, the finite energy

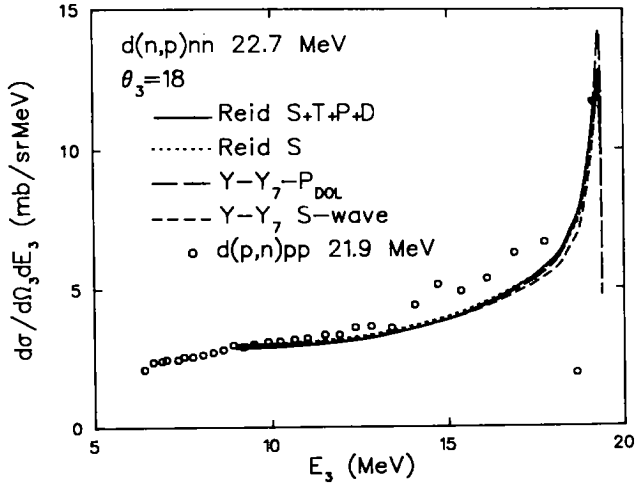

Fig. 20. Breakup differential cross section at 22.7 MeV for the proton spectrum at $\theta_3 = 18°$ for the full Reid and $Y\text{-}Y_7\text{-}P_{DOL}$ potentials and their s-wave truncations.

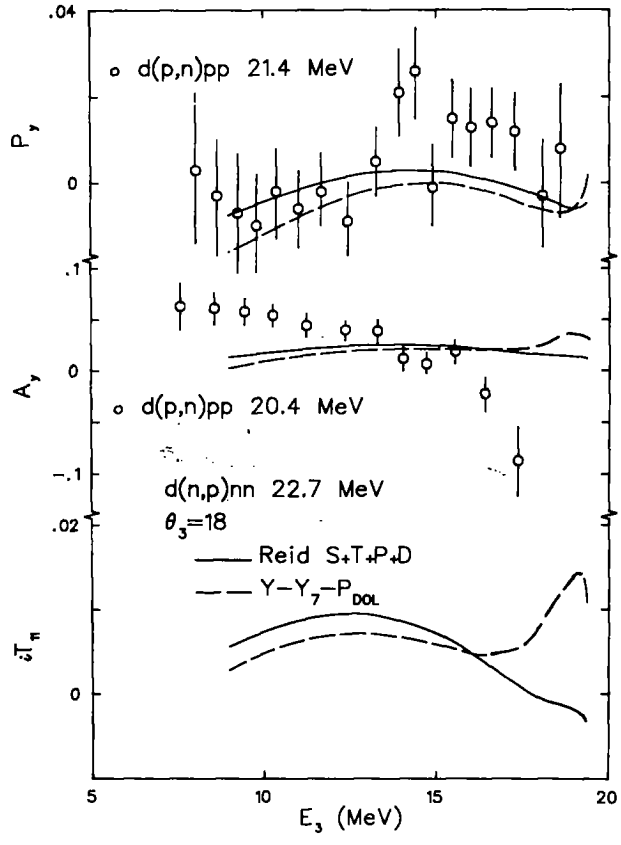

Fig. 21. Vector polarization and analyzing powers corresponding to fig. 20.

resolution in the experiment, and perhaps Coulomb effects. There is little or no influence of the higher partial wave forces on the cross section. The proton polarization (fig. 21) is very small, and shows little resemblance to the corresponding experimental neutron polarization [28]) at 21.4 MeV. Also the perturbational and exact results for the Y-Y_7-P_{DOL} potential [8]) do not coincide. For the neutron and deuteron vector analyzing powers the situation is more or less the same; for the Y-Y_7-P_{DOL} potential the exact results for iT_{11} are approximately 0.005 below our perturbational results for all energies E_3.

Results for the symmetric-constant-relative-energy locus and for the FSI locus at 22.7 MeV were published in our letter [12]). We recall that at this energy the FSI results display a strong dependence on the magnitude and direction of the relative momentum of the outgoing n-p pair.

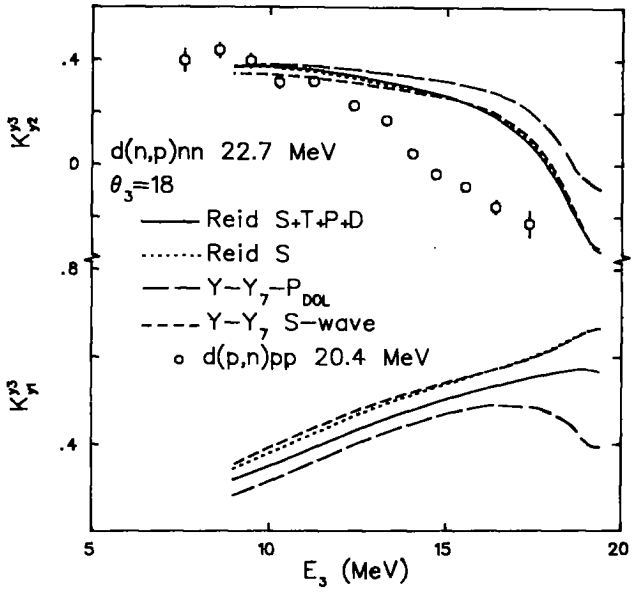

Fig. 22. Vector polarization transfer coefficients corresponding to fig. 20.

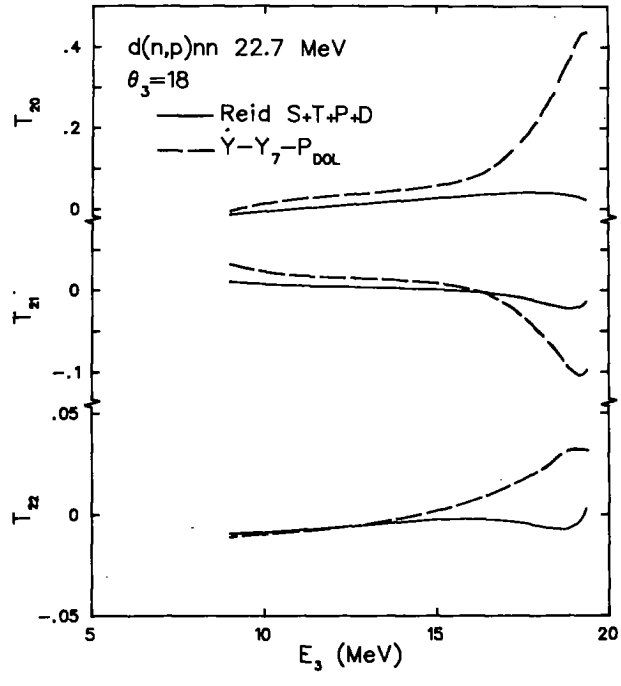

Fig. 23. Deuteron tensor analyzing powers corresponding to fig. 20.

6. Conclusions

The present work essentially corroborates the conclusions on the validity of the perturbational approach that were drawn from the elastic scattering results: at lower energies the convergence is doubtful, although useful information on the sensitivities may be obtained, and at higher energies the convergence improves, even though the perturbational contributions increase relative to the unperturbed part.

For a general potential one way of checking the convergence of the perturbation series is to compare results for the T-matrix method and the K-matrix method. If also the breakup is calculated, it becomes possible to obtain second-order perturbation terms for the elastic scattering. This possibility has not been implemented in our computer codes, since we first compared to the available exact results as a direct check on the convergence. Also the effort to incorporate this feature should not be underestimated, as it brings in the recoupling function ${}_i\langle pq\Gamma|p'q'\Gamma'\rangle_j$ in its most general form.

Even more than in the elastic scattering the present results indicate that for several observables the two-nucleon d-wave forces are as important as the tensor or p-wave forces.

Our results at 46.3 MeV for the two different realistic potentials show significant differences. To a large extent these can be ascribed to the s-wave parts of the potentials, and in some cases to the different deuteron d-state probability generated by the tensor forces. It should however be noted that the potentials considered also differ with respect to their on-shell behaviour. In view of the found large differences it would be interesting to study at these energies genuine phase equivalent potentials to separate the on- and off-shell effects from each other.

When we compare our breakup scattering results with the available data, we generally find a reasonable agreement for the differential cross section. For the polarization quantities the situation is less clear. At the higher energy our results are not in conflict with the single available set of data, but the uncertainty in the latter is so much larger than the calculated polarization, that no further conclusions can be drawn. At 22.7 MeV our results do not agree with the experiment for the FSI configuration [29]), but there are indications that at this energy the perturbation treatment is not sufficiently converged, and the experimental energy spread is ignored in our results.

The calculated polarizations and analyzing powers in general are rather small, or have larger values only where the cross section is small. An exception is formed by the tensor analyzing powers in some configurations, in particular the FSI; here experiments might be feasible and could give interesting results, although one should also consider the effect of a finite energy resolution. Also the polarization transfer variables have appreciable values; since these are determined mainly by the s-wave forces, their primary usefulness is as information additional to the cross sections.

We thank J. Bruinsma for several discussions and for providing us with numerical details of his calculations.

References

1) R. Aaron, R. D. Amado and Y. Y. Yam, Phys. Rev. **140** (1965) B1291;
R. Aaron and R. D. Amado, Phys. Rev. **150** (1966) 857
2) R. T. Cahill and I. H. Sloan, Phys. Lett. **31B** (1970) 353; **33B** (1970) 195
3) I. H. Sloan, Nucl. Phys. **A168** (1971) 211
4) W. M. Kloet and J. A. Tjon, Ann. of Phys. **79** (1973) 407; Nucl. Phys. **A210** (1973) 380
5) D. D. Brayshaw, Phys. Rev. **D8** (1973) 952; Phys. Rev. Lett. **32** (1974) 382; **34** (1975) 1478
6) M. I. Haftel and E. L. Petersen, Phys. Rev. Lett. **33** (1974) 1229; Proc. Int. Conf. on few body problems in nuclear and particle physics, ed. R. J. Slobodrian *et al.* (les Presses de l'Université Laval, Quebec, 1975); Phys. Rev. Lett. **34** (1975) 1480
7) P. Doleschall, Phys. Lett. **38B** (1972) 298; **40B** (1972) 443; Nucl. Phys. **A201** (1973) 264; **A220** (1974) 491
8) J. Bruinsma, thesis Vrije Universiteit (Amsterdam 1976);
J. Bruinsma and R. van Wageningen, Nucl. Phys. **A282** (1977) 1
9) C. Stolk and J. A. Tjon, Nucl. Phys. **A295** (1978) 384
10) R. V. Reid, Ann. of Phys. **50** (1968) 411
11) L. Črepinšek *et al.*, Acta Phys. Austr. **42** (1975) 139
12) C. Stolk and J. A. Tjon, Phys. Rev. Lett. **39** (1977) 395
13) C. Stolk, thesis Rijksuniversiteit Utrecht (Utrecht 1978)
14) G. G. Ohlsen, Rep. Prog. Phys. **35** (1972) 717
15) H. H. Barschall and W. Haeberli, ed., Polarization phenomena in nuclear reactions (University of Wisconsin Press, Madison 1971) p. xxv
16) K. Watson, Phys. Rev. **88** (1952) 1163
17) J. Gillespie, final state interactions (Holden-Day, San Francisco, 1964
18) T. Y. Wu and T. Ohmura, The theory of scattering (Prentice Hall, Englewood Cliffs, NJ, 1962)
19) M. Jain *et al.*, Phys. Rev. Lett. **31** (1973) 838
20) W. T. H. van Oers, in few body dynamics, ed. A. N. Mitra *et al.* (North-Holland, Amsterdam, 1976) p. 746
21) J. M. Lambert *et al.*, Phys. Rev. **C13** (1976) 43
22) E. L. Petersen *et al.*, Phys. Rev. **C9** (1974) 508
23) M. I. Haftel *et al.*, Nucl. Phys. **A269** (1976) 359
24) D. J. Margaziotis *et al.*, Phys. Rev. **171** (1968) 1170
25) A. S. Clough *et al.*, Nucl. Phys. **A121** (1968) 689
26) P. Leleux, private communication
27) R. G. Graves *et al.*, Phys. Rev. Lett. **35** (1975) 917
28) F. N. Rad *et al.*, Phys. Rev. **C8** (1973) 1248
29) F. N. Rad *et al.*, Phys. Rev. Lett. **35** (1975) 1134